



Soil liquefaction in seasonally frozen ground during the 2016 Mw6.6 Akto earthquake



Yuan Yao^{a,b,*}, Jie Chen^b, Tao Li^c, Bo Fu^b, Haoran Wang^b, Yuehua Li^b, Hailiang Jia^d

^a Earthquake Agency of the Xinjiang Uygur Autonomous Region, Xinjiang, Urumqi 830011, China

^b State Key Laboratory of Earthquake Dynamics, Institute of Geology, China Earthquake Administration, Beijing 100029, China

^c School of Earth Science and Geological Engineering, Sun Yat-Sen University, Guangzhou 510275, China

^d School of Architecture and Civil Engineering, Xi'an University of Science and Technology, Xi'an 710000, China

ARTICLE INFO

Keywords:

2016 Akto earthquake
Frozen soil liquefaction
Liquefaction mechanics
Kongur extension system

ABSTRACT

Soil liquefaction is a type of coseismic hydrological change triggered by earthquakes, and its occurrence results in major property damage and casualties. The dynamics of coseismic hydrological changes are not fully understood. In order to address this, we studied coseismic deformations such as liquefaction and ground fissures that occurred as a result of strong seismic activity during the 2016 Mw6.6 Akto earthquake, which took place in the interior of the Pamir Plateau in northwestern China. This paper presents a systematic survey of the frozen soil liquefaction and ground fissures caused by this earthquake. The majority of liquefaction sites near the Karaat River are located on the T1 terrace, in Bulake village, and are adjacent to the alluvial fan of the Kungai Mountain. We find that the liquefaction was caused by the original spring and coseismic ground fissure during the earthquake. Approximately 80% of the liquefaction sites are formed along the original spring in the epicenter. The maximum height of sand boils is 15 cm. The remaining 20% of the liquefaction sites are formed along the coseismic ground fissure. Our results suggest that the frozen soil layer impedes liquefied material in the lower unfrozen soil layer from reaching the surface, and the material formed from liquefaction is consequentially channeled through the primary fault and coseismic ground fissures. Liquefaction associated with the Akto earthquake demonstrates the importance of accounting for the possibility of a series of coseismic geological disasters, such as soil liquefaction and ground fissures, in areas with similar geology, altitude, and temperature.

1. Introduction

Seismic geological disasters, which are direct disaster earthquakes, include landslides, collapse, ground fissures, debris flows, liquefaction, surface subsidence, and tsunamis. This type of disaster results in heavy casualties and property loss. In general, higher intensity earthquakes trigger stronger geological disasters with wider ranges. This is especially true of earthquakes in mountain areas, such as the 2008 Wenchuan Ms8.0 [30,31,35,37] and the 2010 Qinghai Yushu Ms7.1 earthquakes [36], which caused massive earthquake geological disasters in the meizoseismal area [34] and formed several potential geological disaster areas. Therefore, investigating seismic geological hazards and areas with potential for geological hazards is an important

aspect of seismic site assessment work.

Sand liquefaction is a common earthquake and geological hazard [1,10,12,24,29] wherein seismic waves generated at the source are propagated outward, resulting in an increase in the pore water pressure of the surrounding loose sediment and a loss of soil strength. Thus far, sand liquefaction has been identified in numerous earthquake sites, such as the 1964 New Japan Mw7.5 earthquake [13], 1989 Platts Mw6.9 earthquake [26], and the 1999 Mw7.5 earthquake in Central Taiwan [28,6] Data from these cases have provided insight into the process of earthquake-induced liquefaction, and detailed studies on earthquake-induced liquefaction events have increased with the occurrence of large earthquakes in modern times. However, coseismic hydrological changes are still poorly understood and researchers cannot

* Corresponding author at: Earthquake Agency of the Xinjiang Uygur Autonomous Region, Xinjiang, Urumqi 830011, China.
E-mail address: yy8096658@126.com (Y. Yao).

fully explain the complexity of observed liquefaction events.

Studies [2,33,4] have shown that the phenomenon of sand liquefaction in frozen soil areas occurs in medium-fine sand in the lower part of frozen soils, i.e. in seismic deformation zones near valleys and lakeshores. A sand boil (sand volcano) consisting of ice and sand is formed after the earthquake. The liquified material is about 3 m underground, and the material of liquefaction travels through channels

(ground fissure and pore) to the surface.

This study presents a descriptive case study of the liquefaction and ground fissure in the Pamir Plateau during the 25 November 2016 Mw6.6 Akto earthquake. The relationship between sand liquefaction and ground fissures is analyzed, and the seasonal frozen soil area is discussed.

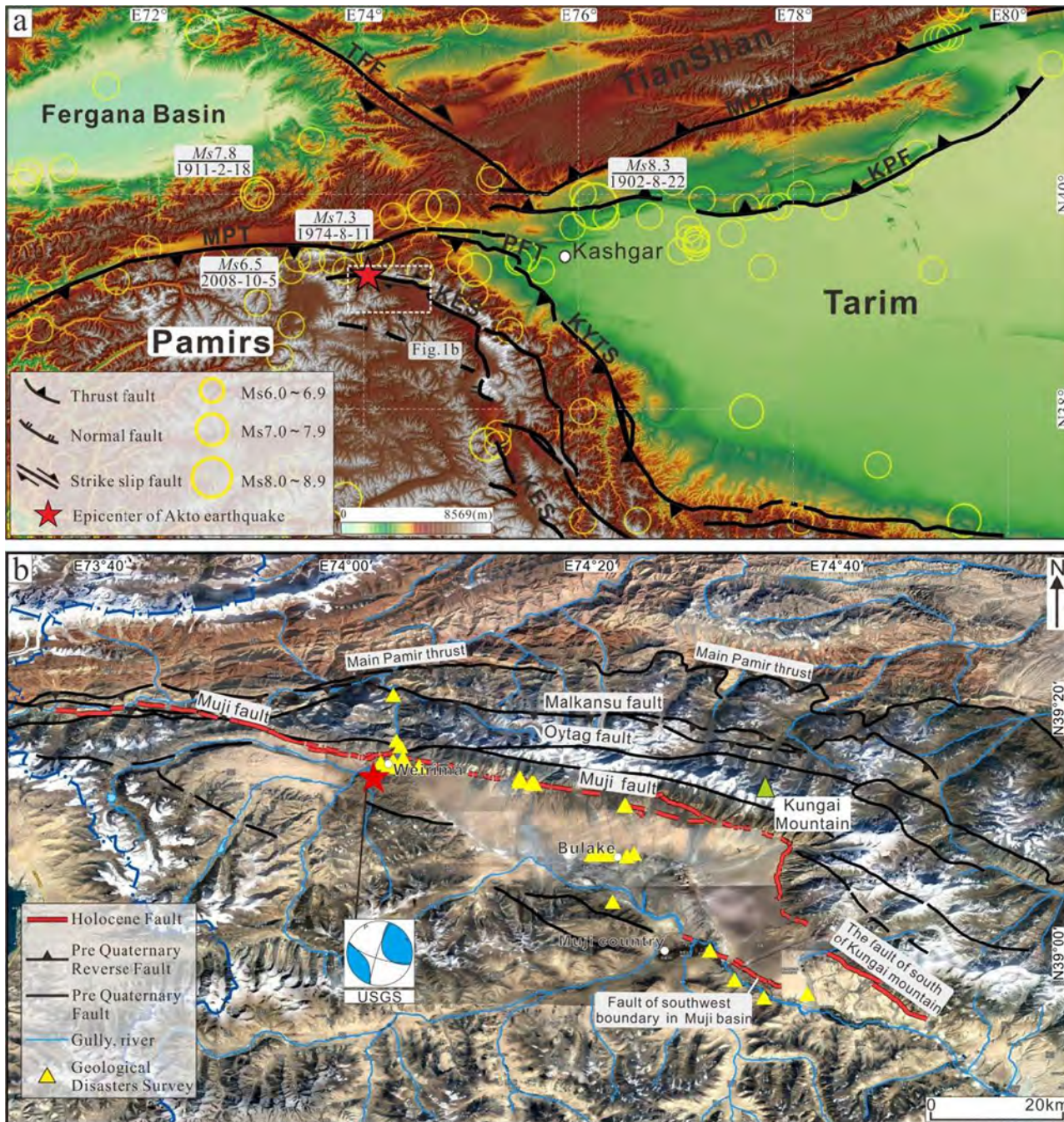


Fig. 1. Topographic and tectonic map of the Muji fault. (a) Geological structure map of the Western Pamirs. The locations of faults were obtained from the Chinese Active Fault Map published in 2004. Earthquake locations were taken from the China Earthquake Networks Center seismic catalog for the $M > 6.0$ records. (b) Seismic geological survey of the 2016 Akto earthquake in map view, see location in inset map (a). The red star indicates the epicenter of the earthquake. Other major faults are shown in black. The yellow triangles indicate potential coseismic geological disaster sites. MPT: Main Pamir Thrust; PFT: Pamir Frontal Thrust; KYTS: Kashgar-Yecheng Transfer System; KES: Kongur Extension System; TFF: Talas Ferghana Fault; KPF: Keping Fault; MDF: Maidan Fault.

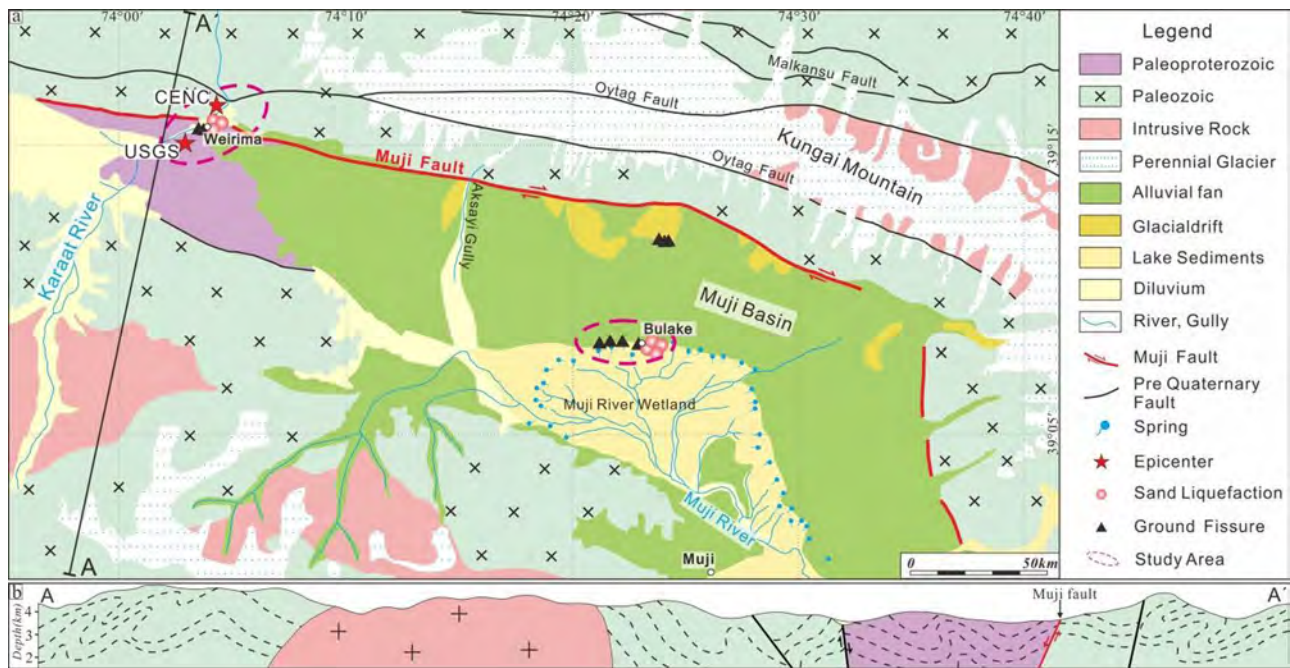


Fig. 2. (a) Geological structure map of the Muji basin. Red lines mark the geological structure of the 2016 Akto earthquake. (b) The cross-section along A–A' shows the fault system and stratigraphy.

2. Materials and methods

2.1. Study location

The Pamir is located in the northwestern corner of the Indo-Asian collision zone. During the late Cenozoic, the northern margin of the Pamir indented northward ~ 300 km, accommodated by south-dipping intracontinental subduction along the Main Pamir Thrust (MPT) and coupled with strike-slip on the western and eastern margins. The Akto Mw6.6 earthquake occurred at the intersection of the Kongur extension system (KES) and the Pamir thrust nappe structure, which is one of the two tectonic junctions caused by the collision of the Indian and Eurasian plates [21,3,32]. The region is one of the most tectonically active areas in the Chinese mainland with a record 17 earthquakes of $M_w \geq 6.0$ having occurred within 100 km of the epicenter. Geospatial data [20,39,40] from this region show that the rate of northward pushing in the region is up to 23 cm/yr. The movement is characterized by crustal shortening and strike-slip, while the deformation is caused by extension movement. In this zone, a series of arcuate tectonic belts that protrude north have been formed, including the Main Pamir Thrust (MPT), Fault-Kashgar-Yecheng Transfer System (KYTS), Pamir Frontal Thrust (PFT) [15], and Kongur extension system (KES) (Fig. 1a). The 2015 Nepal Ms8.0 earthquake was followed by the 2015 Hindu Kush Ms7.8 earthquake, Tajikistan Ms7.4 earthquake [19], and the 2016 Afghanistan Ms7.1 earthquake. It is unknown whether this series of devastating earthquakes was related to the 2015 Nepal Ms8.0 earthquake. The seismogenic layer of this earthquake was determined to be on the Muji fault zone, in the northeastern margin of the Muji Basin. The fault is located at the northern end of the Kongur extension system [14,16,22,23,27,5,7].

The Muji Basin belongs to the fault depression basin of the Pamir Plateau. The average elevation exceeds 3300 m (Fig. 1b) and the average winter temperature, a result of the interaction between soil and

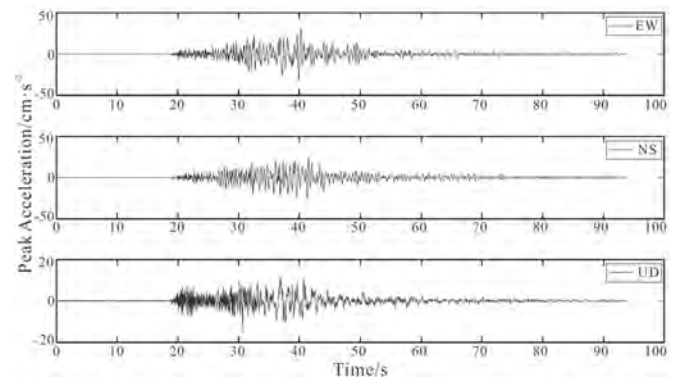


Fig. 3. Peak accelerating records after correction of Jigen station. These data are measured by strong motion seismograph. The three figures are peak acceleration in different direction.

air temperature, is about -10 °C [38]. Soil thaws in the spring when the average temperature exceeds 0 °C, then freezes when the winter temperature drops below 0 °C, resulting in sandy liquefaction of a large area in the permafrost zone. Although the Akto Mw6.6 earthquake was relatively small, it still induced range sand liquefaction.

The Muji fault (Fig. 2a) is the transitional fault at the northern end of the Kongur extension system. It is more than 100 km long, with a NW strike and the NE tendency. The fault exhibits a dextral strike [22,5]. A clear fault facet has developed along the fault, with moraine deposits and gullies broken to the right. The largest recorded earthquake in the Muji fault was the Tashkurgan Ms7.0 earthquake on July 5, 1895. The earthquake formed a 27 km long earthquake surface rupture zone [14,8]. The alluvial fan and river system were broken by the Muji fault,

Table 1
A summary of field observations and measurements of sand liquefaction.

Site No.	Longitude (°)	Latitude (°)	DSV (m)	DS (m)	FL (m)	ASV	Material
1	39.260481	74.064797	0.9		25	1	
2	39.260503	74.064854	0.2		20	1	
3	39.260575	74.064973	1		12	1	
4	39.260718	74.064993	0.3		30	1	
5	39.260691	74.065328	0.3		5	1	
6	39.260638	74.065454	1		8	1	Black mud and silt
7	39.260423	74.065785	0.5	5		1	Gray-black silt
8	39.260579	74.065823	0.4	5		1	
9	39.260625	74.065925	0.5	3		1	
10	39.260631	74.066035	0.4	3		1	
11	39.260590	74.065976	0.3	1.7		3	
12	39.260675	74.065947	0.15	4.3		5	
13	39.260763	74.066076	0.4	4		5	
14	39.260784	74.065973	1	3.6		1	Gray-yellow silt and sand
15	39.260715	74.066071	0.8	3		3	
16	39.260861	74.066056	0.1	4		10	
17	39.260805	74.066043	0.1			6	
18	39.260837	74.065941	0.3	4		1	
19	39.260919	74.065970	0.1	3.5		14	
20	39.261026	74.066115	0.05	5		100	
21	39.261063	74.065997	0.1	2		10	
22	39.260975	74.065998	0.1	5		105	
23	39.260997	74.065890	0.05			52	
24	39.261221	74.065916	0.2	5		1	
25	39.261291	74.065872	0.05	4.6		30	
26	39.261146	74.065695	0.05	3.7		10	
27	39.261091	74.065675	0.1			3	Gray-green silt
28	39.261195	74.065238	0.1		5	3	

Site No.: number assigned during field investigation (see Fig. 3a); DSV.: diameter of sand volcano; DS: diameter of spring; FL: fissure length; ASV: amount of sand volcano (There are some small sand volcano, and we have counted it. The characteristic of sand volcano are show in Fig. 7.).

forming a clear fault scarp to the west of the epicenter and a large fault trough to the east. Multiple secondary faults connected two sections of the main fault. The structure of this event has resulted in tensile stress and compressive stress coexisting in this region.

The Mw6.6 Akto earthquake occurred at 14:24:30 UTC on November 25, 2016, in Akto County, Xinjiang Autonomous Region. The epicenter was located at 39.27°N, 74.04°E, with a focal depth of 10 km (<http://www.cea.gov.cn/publish/dizhenj/464/15/20161125231007712890916/index.html>). Inversion of the source mechanism showed it to be a strike-slip earthquake. The epicenter of the earthquake was near the Weirima village beside the Kalate River, about 165 km from the town of Akto and 3700 m above sea level. The lowest temperature is -22°C and the average temperature is -13°C in the study area. As of December 7, 2016, 734 aftershocks were recorded, two of which were Ms5.0–5.9 and 35 were Ms4.0–4.9. The maximum aftershock was Ms5.1. The nearest strong ground motion station (Jigen station) is 58 km away from the epicenter, and the maximum peak acceleration of 31.3 cm/s^2 (Fig. 3). The aftershocks were mainly distributed along the south of the fault. The earthquake caused many secondary geological disasters, such as soil liquefaction, ground fissures, collapse, and landslides. The liquefaction and ground fissure were responsible for the majority of property damage in the region.

2.2. Investigation of liquefaction and ground fissure

Surveys were conducted a few days after the earthquake (from November 27 to December 1). We focused on two study areas: the epicenter (Weirima village) and Bulake village (Fig. 2). The Weirima

study area contains one river, the Karaat (Fig. 2), and the lowest terrace risers are generally located along river channels, around 1.0–3.0 m above the current river bed. The Bulake study area is located at the boundary of the alluvial fan and Muji River wetland. Differential GPS (HITARGET IRTK, precision in floating mode is 0.015 m) and an unmanned aerial vehicle (UAV) (DJI, inspire 1 and ZENMUSE X3 camera with 12 million pixels) were used to obtain distribution data of liquefaction and ground fissure in these two study areas. The survey was conducted in linear paths along the ground fissure (Table 2), and liquefaction was measured in the form of points (Table 1). Second, the photos (about 50–100 photos) taken by the UAV at a height of 100 m were spliced to obtain the latest image of the two study areas. Finally, the distribution data of liquefaction and ground fissure was superimposed on this image (Figs. 4a, 5a, 6a). To identify the source and formation mechanism of sand liquefaction at the epicenter, a trench excavation was carried out at the edge of the sand boil (Fig. 4b). The composition and color of the material from the surface was compared with materials from different depths to identify the layer from which the material originated.

3. Results

3.1. Sand liquefaction

Different types of sand liquefaction were observed in the villages of Weirima and Bulake.

Table 2
Measurements of ground fissures in the Bulake study area.

Site No.	1	2	3	4	5	6	7	8	9	10	11	12	13	14	15	16	17	18	19	20	21	22	23	24	25	26	27	28	29	30	31
FW	15	15	15	17	12	12	11	13	10	12	10	12	12	6	30	41			15	12	8	25	27	7	80	30	20	12	15	11	11
FD	39	120	68	70	50	50	40			78	78	57	57	57	57	76			55	78	45	54	60		53	65	67	38	22	46	
VM	6			8	20	6	12	12	10	10	10	30	6	4	3	4	3	16	13	4	14	5	7	11	42	3	10	4	9	9	
Direction	110	110	115	110	140	305	90	90	315	298	115	305	305	120	90	90	95	110	140	95	105	105	110	120	95	95	95	115	80	95	80

Site No.: number assigned during field investigation (see Fig. 6a); FW: fissure width (cm); FD: fissure depth (cm); VM: vertical motion (cm); Direction: the motion direction of extension and strike-slip ground fissures (degree).

3.1.1. Sand liquefaction in the Weirima study area

We found that although most of the sand liquefaction caused by this earthquake occurred in the original fault, the liquefaction that occurred along the ground fissures was another important form. This earthquake caused sand liquefaction around about 20% of the primary faults. The diameter of the mouth forming each boil was about 0.05–0.2 m, with the cone diameter and height measuring about 0.3–1.5 m and up to 15 cm, respectively. The liquefied material was mostly gray-green clay.

We explored a layer of saturated gray-green clay at the depth of 1.8 m (Fig. 4c) and found that the liquefied material was mostly the same. Thus, we can make a preliminarily inference that the liquefied material came from this layer.

3.1.2. Sand liquefaction in the Bulake study area

We found that sand had liquefied in wetland and marsh areas at the intersection of the front edge of a piedmont alluvial fan and the Muji River, 100 m east of Bulake village. The average temperature of the region is below -15°C , which causes the surface to freeze and hide the direct evidence of sand liquefaction. However, we found several new water gushing and freezing phenomena. As a large area of ice had formed on the surface, water sprays and sand were ejected along the meadow roots and froze quickly. Evidence of sand boils exist under the ice, as a series of circles formed because of the thick ice layer.

3.2. Ground fissures

Many ground fissures were formed on the surface of the two study areas during the earthquake. These fissures were distributed across the flood plain, terrace, and alluvial fan of the Karaat River (Figs. 5 and 6).

Ground fissures covering a large area were found on the flood plain of the river, on the western side of the epicenter. These ground fissures were distributed in a chessboard pattern (Fig. 5a, b); the widths of the cracks were almost the same, which made it difficult to distinguish between primary and secondary fissures. The NS and EW ground fissures grew equally on the eastern side of the flood plain, but those on the southern side were mainly in the EW direction. These fissures were formed mainly by extensional movements, although a few of them were caused by strike-slip displacement.

The ground fissures that formed on the T1 terrace of the Karaat River are distributed linearly, and there were clearly fewer of them at this site than on the flood plain. The primary and secondary ground fissures could be clearly differentiated here. The width of the ground fissures on the terraces was 10–15 cm and they were 1 m deep (Fig. 5c).

According to the field investigation (Fig. 6a), the ground fissures to the east of Bulake village were mainly tensile and strike-slip structures (Fig. 6e, f). The maximum width and depth of the SN ground fissures were 41 and 76 cm, respectively (Fig. 6b, d). The EW ground fissures are mainly sinistral-slip, at angles of $298\text{--}315^{\circ}$ (Fig. 6c). Examining the dominant directions of motion of the tensile and strike-slip ground fissures revealed that they were almost the same, distributed between 90° and 135° (Fig. 6c) in a circular pattern. Statistical analysis showed that the ground fissures were mostly 60–75 cm deep, which directly reflected the thickness of the frozen soil layer. The width of the ground fissures averaged 17 cm.

4. Discussion

4.1. Sand liquefaction in frozen soil

Sand liquefaction generally happens in the sandy soil layer, in a state between saturation and semi-saturation. The thickness of the frozen soil layer was about 1 m at the epicenter of the Akto earthquake,

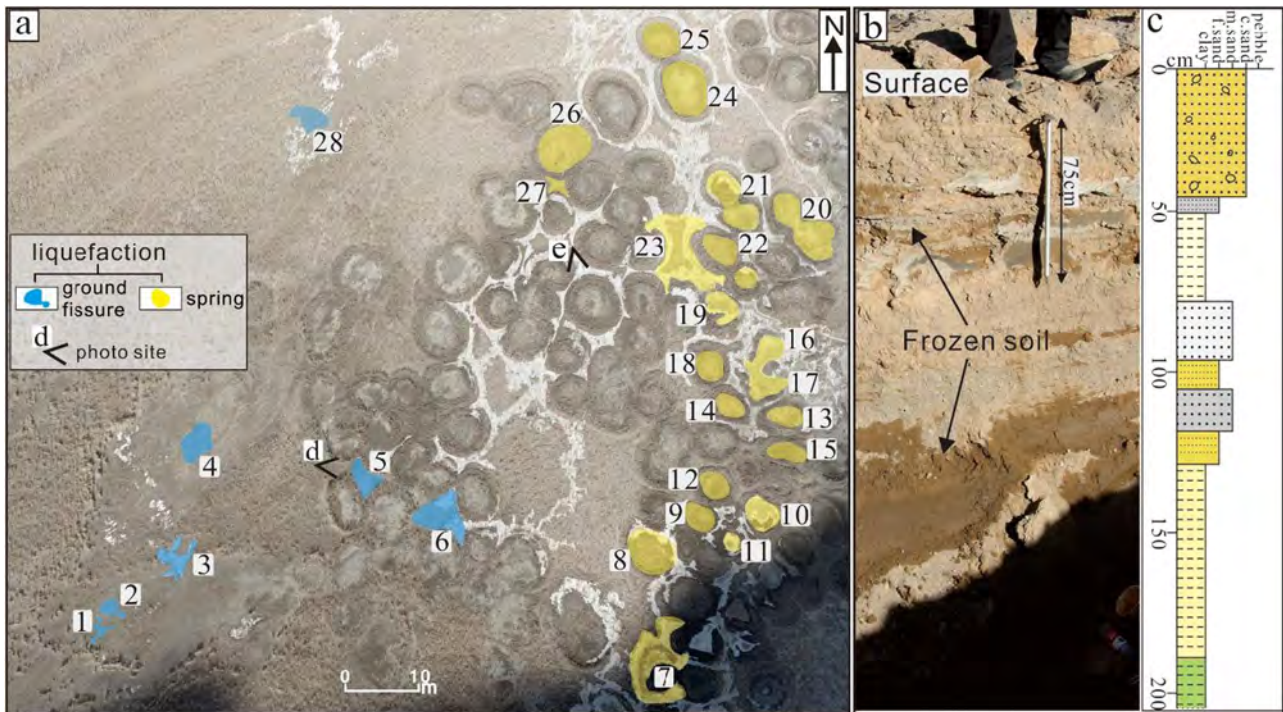


Fig. 4. (a) Sand liquefaction around the earthquake epicenter. Blue areas indicate liquefaction along the coseismic ground fissure; yellow areas indicate liquefaction along the original fault. The number in the (a) map is the identifier of the measurement points (see Table 1). (b) The trench at the epicenter. (c) The stratigraphic histogram of the trench shown in (b).

and sand liquefaction occurred under the frozen soil layer. This raised the question of whether liquefaction occurred in the lower foundation layer, despite the fact that sand boils do not typically appear in similar regions after earthquakes.

The majority of the sand liquefaction at the epicenter formed along the primary faults, and this was one of the main reasons why large-scale sand liquefaction was caused by this earthquake. Further study could reveal the mechanism that formed these primary faults and if they were produced by ancient seismic activity, which could have released energy dozens of times that of the Mw6.6 earthquake. Furthermore, the area is located near the Muji fault. Therefore, the possibility of large future earthquakes causing sand liquefaction merits further study.

The sand liquefaction in the seasonal frozen soil area differs from that in other areas; the frozen layer extends under the surface, and a large area of the lower frozen soil layer was liquefied with the vibration. The liquefaction occurred in an area about 1000 m² around the epicenter. The frozen soil layer on the surface obstructed the liquefied material in the lower soil layer from rising to the surface. Therefore, the liquefied sand material could only be forced upwards through existing channels (e.g., springs, ground fissures, meadow root systems).

4.2. Relationship between ground fissures and sand liquefaction

Two types of liquefaction occurred in the frozen soil layer during this earthquake (Fig. 8): that which occurred along the original fault (Fig. 10d) and that which formed along the ground fissures (Fig. 10c). The results of our field investigation allowed us to conduct a preliminary analysis of the formation mechanism of these two types of

liquefaction. The sand liquefaction that occurred along the original fault showed that channels were present in the former after the surface froze, and that the sand liquefaction occurred in a layer of unfrozen soil below the layer of frozen soil (Fig. 8a). After the earthquake, the liquefied sand reached the surface along the fault channel (Fig. 8b).

The sand liquefaction that occurred along the ground fissures showed that there was a certain thickness of unfrozen soil under the frozen soil layer (Fig. 8c). During the earthquake, the material in the unfrozen soil layer was liquefied, emerged along the ground fissures, and finally reached the surface (Fig. 8d). We speculate that the frozen soil layer impedes the liquefied material in the lower unfrozen soil layer from reaching the surface, and that the original fault and coseismic ground fissures were used as channels instead. This enabled the onset of liquefaction in the uppermost aquifers, which tended to be dominated by loose sandy gravel material. This mechanism was previously theorized by Wang [29].

4.3. Determining the thickness of the frozen soil layer

From our field investigation, we inferred that sand liquefaction occurred mainly along the fault, but also that a small amount of sand liquefaction occurred along ground fissures. The same sand liquefaction phenomenon was also found at the site of the 2001 Ms8.1 Kunlun Mountain earthquake [4]. It can be concluded that the sand liquefaction that occurred along the ground fissures revealed the characteristics of sand liquefaction in the frozen soil areas. The action of the earthquake causes the pore water pressure in unfrozen soil to increase, which causes sand liquefaction. However, as the liquefied material is unable to

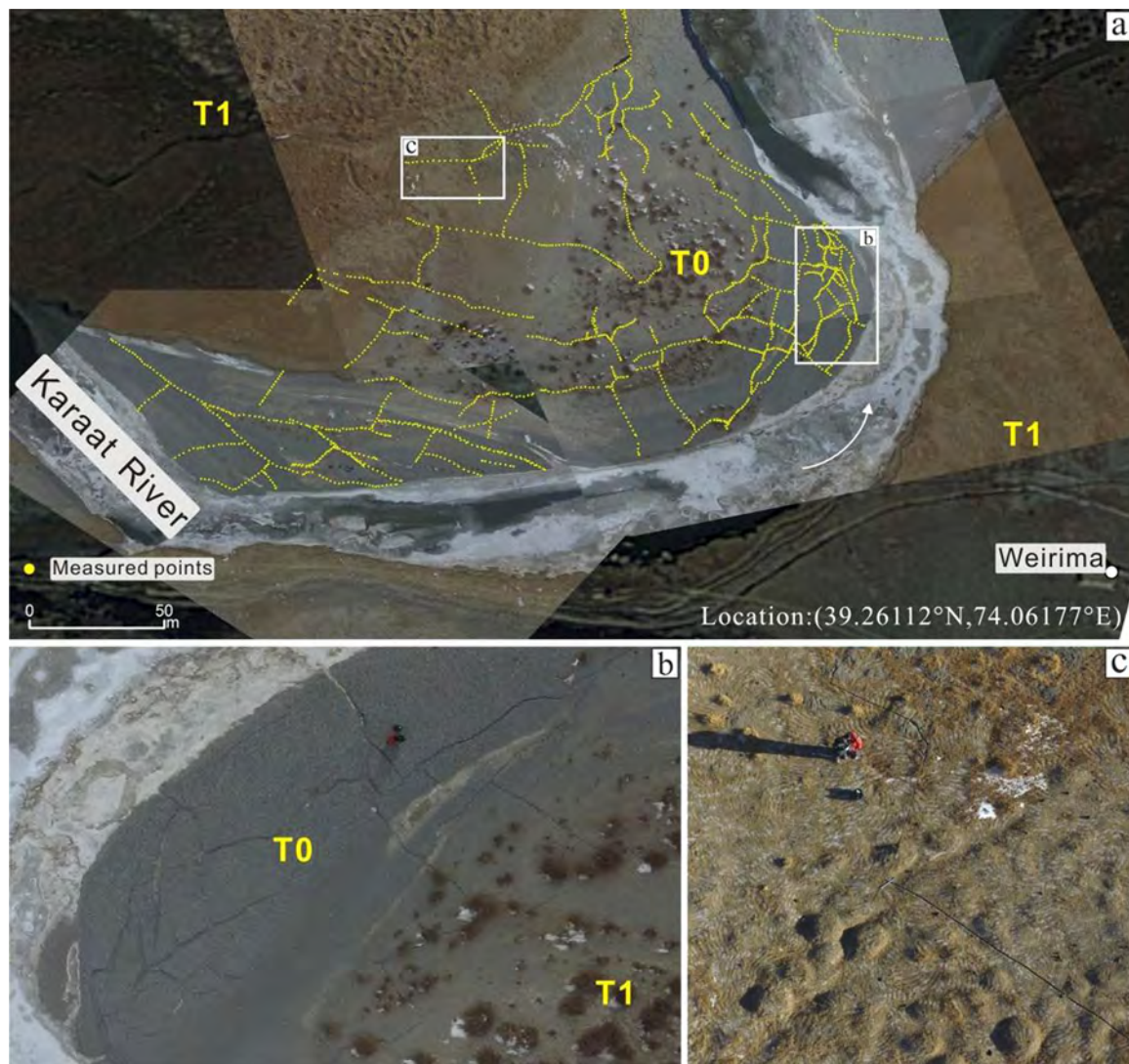


Fig. 5. (a) Coseismic ground fissures at the earthquake epicenter, measured by a differential GPS and an UAV. The background-image is a Google Earth image and high-brightness images were taken by an UAV. The yellow points are the points measured by the differential GPS. (b) The ground fissures in the floodplain, distributed in a chessboard pattern. (c) The ground fissures in the terrace, distributed linearly.

break through the frozen soil, it can only pass through existing channels to reach the surface. This mechanism shows that the thickness of the frozen soil layer in a region is equal to the depth of the ground fissures present.

To determine the thickness of the frozen soil layer, we measured the depth of the ground fissures in Bulake village. These depths were mainly distributed in the range of 60–75 cm, with the thickness decreasing from west to east along the topographic slope. Based on the statistical data on the ground fissures, we used software (Surfer 8 and ArcMap 10.2) to generate the distribution map of frozen soil depth at Bulake village shown in Fig. 9. The map shows that the thickness of the frozen soil layer gradually decreases from the alluvial fan to the Muji River wetland.

5. Conclusions

In this paper, we present a systematic post-earthquake field

investigation of the Mw6.6 Akto earthquake liquefaction and coseismic ground fissure sites. We have identified areas of unusually intense liquefaction located on terrace T1 of the Karaat River and at Bulake village, adjacent to the alluvial fan near the Kungai Mountain. We found that liquefaction occurred both along the original fault and along coseismic ground fissures during this earthquake. Approximately 80% of the liquefaction sites are along the original fault at the epicenter of the earthquake, where the maximum height of the sand boils are 15 cm. The liquefied material consists of gray-green clay and sand. The remaining 20% of the liquefaction sites were formed along the coseismic ground fissures. Our results suggest that the frozen soil layer impedes the liquefied material in the lower unfrozen soil layer from reaching the surface; therefore, the original fault and coseismic ground fissures are used as channels for the liquefied material. This enables the onset of liquefaction in upper aquifers, which tend to be dominated by loose sandy gravel material.

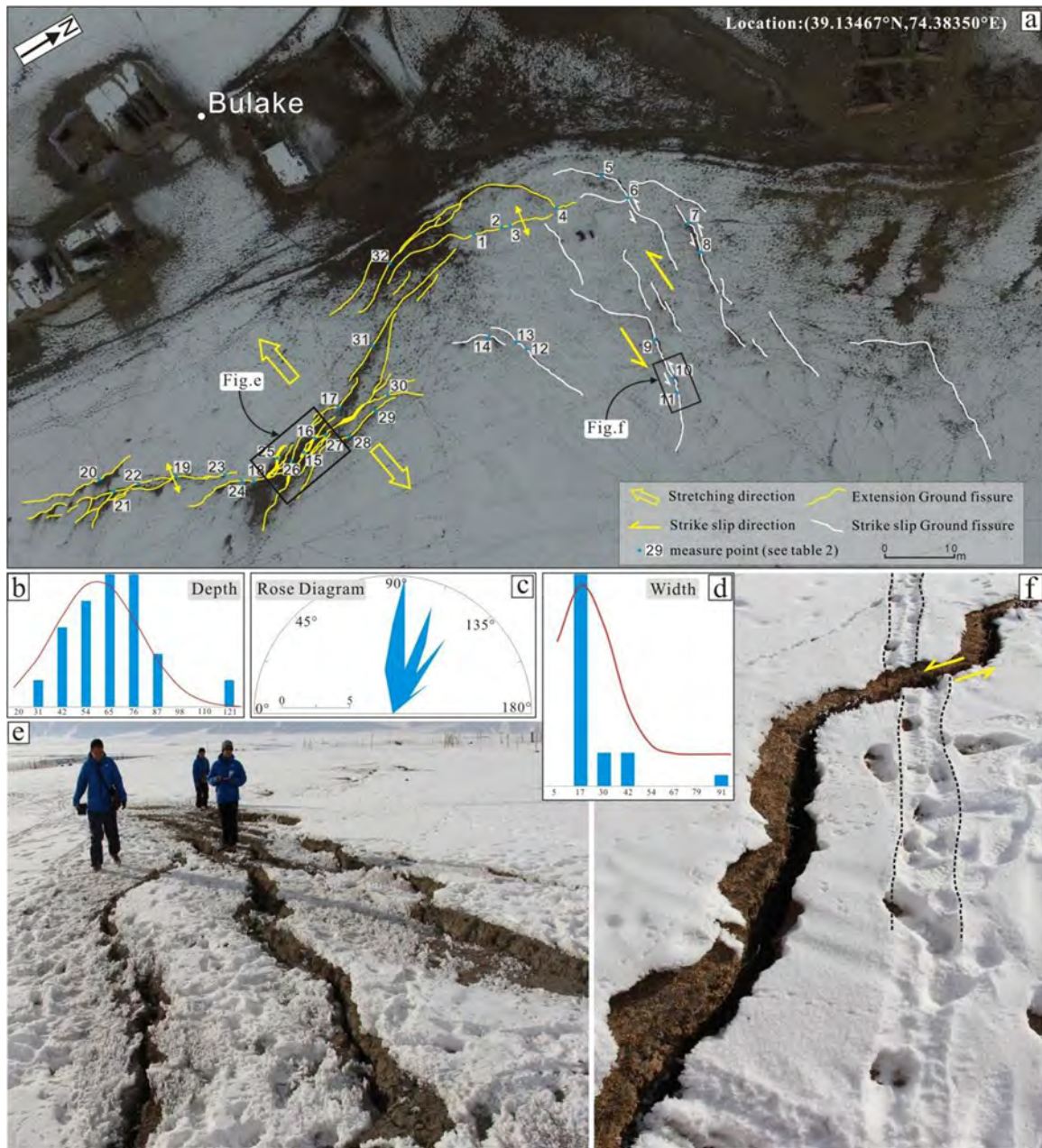


Fig. 6. Characteristics and statistical analysis of ground fissures in the Bulake study area. (a) Yellow and white lines indicate the extension and strike-slip ground fissures, respectively. The number in the (a) map is the identifier of the measurement point (see Table 2). (b), (c), and (d) show different parameters of the ground fissures. (e) and (f) are photographs illustrating the characteristics of the ground fissures.



Fig. 7. Schematic diagram of the related measurement parameters. (a) ASV (Table 1). (b) VM, FD, and FW (Table 2).

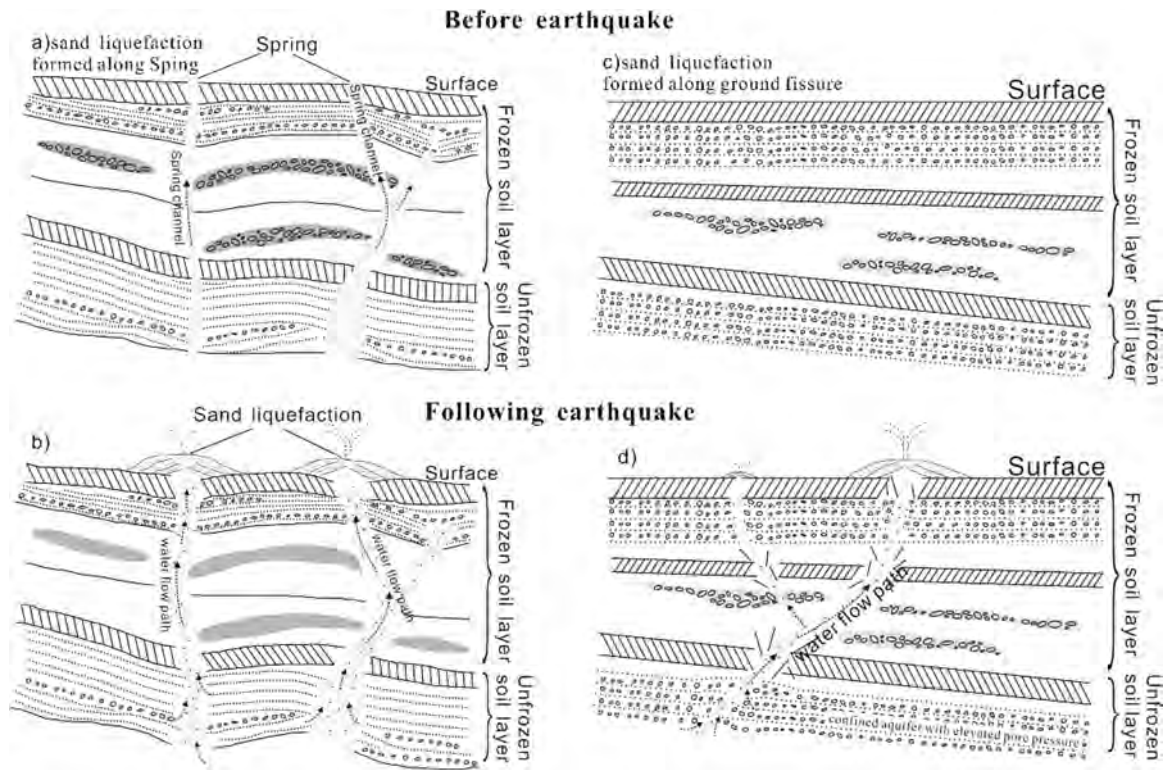


Fig. 8. Schematic diagrams illustrating the conceptual model of the liquefaction of frozen soil during a strong earthquake (Modified from Jing et al., 2016). (a) and (c) illustrate the relationship between the frozen and unfrozen soil layers before the earthquake. (b) and (d) illustrate how sand liquefaction reaches the surface during the earthquake: part of the liquefaction travels along the original faults while the rest passes through the coseismic ground fissures.

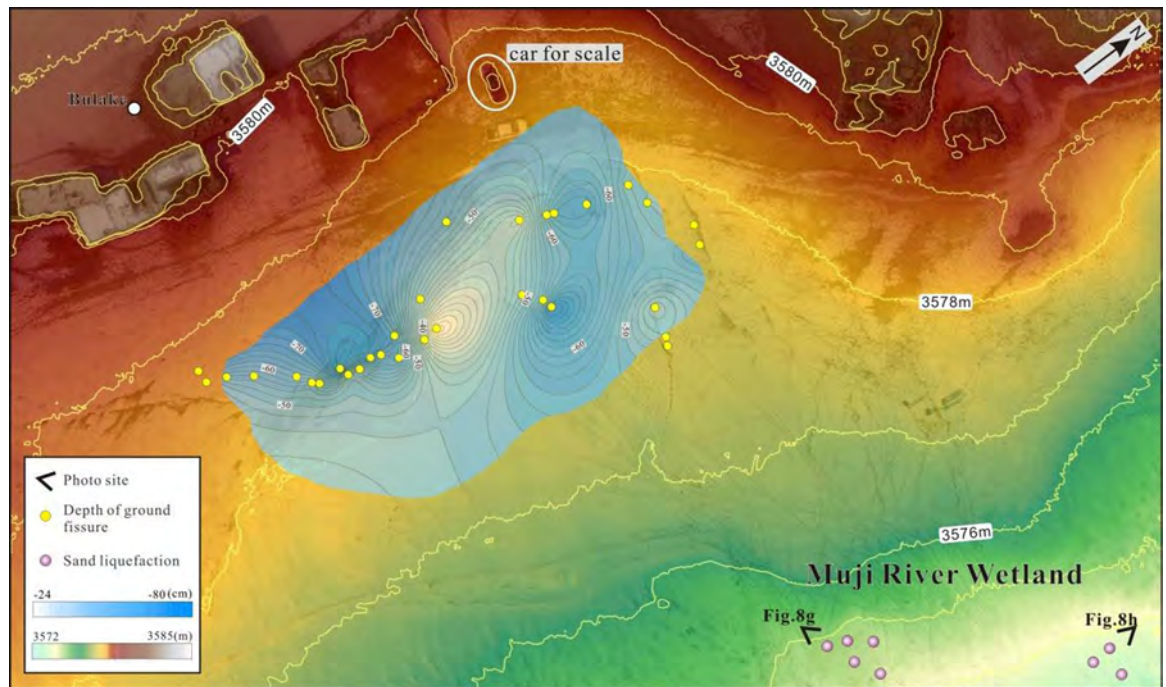


Fig. 9. Contour map (10 cm interval) showing the thickness of the frozen soil layer (blue area) in the Bulake study area. The yellow dots denote the depth of the ground fissure. The background-image is a Digital Elevation Model (DEM) superimposed with the images taken by an UAV.



Fig. 10. Field photographs of this earthquake. (a) The fault scarp of the Muji fault. (b) Coseismic ground fissures in the Bulake study area. (c) and (d) Liquefaction originating from ground fissures in the epicenter. (e) The primary spring at the epicenter. (f) Property damage caused by coseismic ground fissures. (g) and (h) Sand liquefaction in the Bulake study area.

Acknowledgments

This study was supported by Science for Earthquake Resilience of China earthquake administration (XH17042Y), Science and Technology Partnership Program of Shanghai Cooperation Organization (2017E01030) and the National Science Foundation of China (41272195, 41302172, 41374040).

References

- [1] Ambrasey N, Sarma S. Liquefaction of soils induced by earthquake. *Bull Seismol Soc Am* 1969;59(2):651–64.
- [2] Akili W. Stress-strain behavior of frozen fine-grained soils. *High-Way Res Rec* 1971;360:1–8.
- [3] Burtman VS, Molnar P. Geological and geophysical evidence for deep subduction of continental crust beneath the Pamir. *Spec Pap Geol Soc Am* 1993;281(2):248–51.
- [4] Chen YM, Wang LM, Dai W, Wang WF, Dai HG. The frozen soils and devastating characteristics of west Kunlun mountains pass Ms8.1 earthquake area in 2001. *Earthquake research in China*. 20(2):161–169[in Chinese, with English abstract]; 2004.
- [5] Chen J, Li T, Li W, Q, Yuan Z, D. Late Cenozoic and present tectonic deformation in the Pamir Salient, northwest China. *Seismol Geol* 2011;33(2):241–59. [in Chinese, with English abstract].
- [6] Central Geological Survey. Survey Report of Earthquake Central Geological Survey, Survey Report of Earthquake Geology in the 9/21 Chi-Chi Earthquake Taiwan. Taiwan: Central Geological Survey; 2000.
- [7] Coutand I, Strecker MR, Arrowsmith JR, Hillel G, Thiede RC, Korjenkov A, Omuraliev M. Late Cenozoic tectonic development of the intramontane Alai Valley (Pamir–Tien Shan region, central Asia): an example of intracontinental deformation due to the Indo-Eurasia collision. *Tectonics* 2002;21:1053–71. <https://doi.org/10.1029/2002TC001358>.
- [8] Feng XY. The Paleoearthquakes in Xinjiang Region. Urumqi: Sci-Tech and Public Health Press of Xinjiang; 1997. [in Chinese].
- [10] Holzer TL, Jayko AS, Hauksson E, Fletcher JPB, Noce TE, Bennett MJ, Dietel CM, Hudnut KW. Liquefaction caused by the 2009 Olancho, California (USA), M 5.2 earthquake. *Eng Geol* 2010;116(1–2):184–8.
- [12] Ishihara K. Liquefaction and flow failure during earthquakes. *Géotechnique* 1993;43(3):351–451.
- [13] Iwasaki T. Soil liquefaction studies in Japan: state-of-the-art. *Soil Dyn Earthq Eng* 1986;5(1):2–68.
- [14] Li WQ, Chen J, Yuan ZD, Huang MD, Li T, Yu Song, Yang XS. Coseismic surface ruptures of multi segments and seismogenic fault of the Tashkorgan earthquake in Pamir, 1895. *Seismol Geol* 2011;33(2):260–76. [in Chinese, with English abstract].
- [15] Li T, Chen J, Thompson J, A, Burbank D, W, Xiao W. Equivalency of geologic and geodetic rates in contractional orogens: new insights from the Pamir Frontal Thrust. *Geophys Res Lett* 2012;39:L15305. <https://doi.org/10.1029/2012GL051782>.
- [16] Li T. Active thrusting and folding along the Pamir Frontal Thrust System. *Institute of Geology, China Earthquake Administration*; 2012. [in Chinese].
- [19] Metzger S, Schurr B, Ratschbacher L, Schöne T, Zhang Y, Kufner S-K, Sudhaus H. Rupture model of the 2015 M7.2 Sarez, Central Pamir, earthquake and the importance of strike-slip faulting in the Pamir interior. Abstract T11A-2579 presented at 2011 Fall Meeting, AGU, San Francisco, Calif, 12–16; 2016.
- [20] Mohadjer S, Bendick R, Ischuk A, Kuzikov S, Kostuk A, Saydullaev U, Lodi S, Kakar D, M, Wasy A, Khan M, A, Molnar P, Bilham R, Zubovich A.V. Partitioning of India-Eurasia convergence in the Pamir-Hindu Kush from GPS measurements. *Geophys Res Lett* 2010;37:L04305.
- [21] Reigber C, Michel G, W, Galas R, Angermann D, Klotz J, Chen J, Y, Papschev A, Arslanov R, Tzurkov E, T, Ishanov M, C. New space geodetic constraints on the distribution of deformation in Central Asia. *Earth Planet Sci Lett* 2001;191(1):157–65.
- [22] Robinson A, C, Yin A, Manning C, E, Harrison T, M, Zhang S, H, Wang X, F. Tectonic evolution of the northeastern Pamir: constraints from the northern portion of the Cenozoic Kongur Shan extensional system. *Geol Soc Am Bull* 2004;116:953–74.
- [23] Robinson A, C, Yin A, Manning C, E, Harrison T, M, Zhang S, H, Wang X, F. Cenozoic evolution of the eastern Pamir: implications for strain-accommodation mechanisms at the western end of the Himalayan-Tibetan orogen. *Geol Soc Am Bull* 2007;7:882–96.
- [24] Ross G, A, Seed HB, Migliaccio RR. Bridge Foundation behavior in Alaska earthquake. *J Soil Mech Found Div* 1969;95:190–242.
- [26] Sims J, D, Garvin C, D. Recurrent liquefaction induced by the 1989 Loma Prieta earthquake and 1990 and 1991 aftershocks: implications for paleoseismicity studies. *Bull Seismol Soc Am* 1995;85(1):51–65.
- [27] Strecker MR, Frisch W, Hamburger MW, Ratschbacher L, Semiletin S. Quaternary deformation in the eastern Pamirs, Tadjikistan and Kyrgyzstan. *Tectonics* 1995;14(5):1061–79.
- [28] Wang C, Dreger D, S, Wang C, Mayeri D, Berryman J, G. Field relations among coseismic ground motion, water level change and liquefaction for the 1999 Chi-Chi (Mw = 7.5) earthquake, Taiwan. *Geophys Res Lett* 2003;30(17). [HLS1.1-HLS1.4].
- [29] Wang C, Y. Liquefaction beyond the Near Field. *Seismol Res Lett* 2007;78(5):512–7.
- [30] Xu C, Dai F, C, Chen J, Xu X, B, Xu L, Li W, C, Tian W, Cao Y, B, Yao X. Identification and analysis of secondary geological hazards triggered by a magnitude 8.0 Wenchuan earthquake. *J Remote Sens* 2009;13(4):745–62. [in Chinese, with English abstract].
- [31] Xu C, Dai F, C, Xu X, W. Wenchuan earthquake-induced landslides: an overview. *Geol Rev* 2010;56(6):860–74. [in Chinese, with English abstract].
- [32] Yang S, M, Li J, Wang Q. The deformation pattern and fault rate in the Tianshan Mountains inferred from GPS observation. *Sci China Ser D* 2008;51:1064–80. [in Chinese, with English abstract].
- [33] Yang Z, Zhang X. Impact of ground freezing on seismic performance of bridge pile foundations subject to liquefaction-induced lateral spread. *Transp Res Rec* 2017;2656. <https://doi.org/10.3141/2656-08>.
- [34] Yao Y, Hu W, H, Wu G, D, Tan M, Alimujiang, Chang X, D, Luo J. Geological hazard characteristics and seismic intensity of July 3, 2015, Pishan, Xinjiang, Ms6.5 earthquake. *China Earthq Eng J* 2016;38(4):663–8. [in Chinese, with English abstract].
- [35] Yin Y, P. Researches on the geo-hazards triggered by Wenchuan earthquake, Sichuan. *J Eng Geol* 2008;16(4):433–44. [in Chinese, with English abstract].
- [36] Yin Y, P, Zhang Y, S, Ma Y, S, Hu D, G, Zhang Z, C. Research on major characteristics of geohazards induced by the Yushu Ms7.1 earthquake. *J Eng Geol* 2010;18(3):289–96. [in Chinese, with English abstract].
- [37] Yuan X, M, Cao Z, Z, Sun R, Chen L, W, Meng S, J, Dong L, Wang W, M, Meng F, C, Chen H, J, Zhang J, Y, Cai X, G. Preliminary research on liquefaction characteristics of Wenchuan 8.0 earthquake. *Chin J Rock Mech Eng* 2009;28(6):1288–96. [in Chinese, with English abstract].
- [38] Zhou Y, W, Guo D, X, Qiu G, Q. The frozen soil in China. Beijing: science press; 2000. p. 110–34.
- [39] Zubovich A, Wang X, Scherba Y, Kuzikov S, I. GPS velocity field of the Tien Shan and surrounding region. *Tectonics* 2010;29:TC6014. <https://doi.org/10.1029/2010TC002772>.
- [40] Zubovich A, Schöne T, Metzger S, Mosienko O, Mukhamediev S, H, Sharshebaev A, Zech C. Tectonic interaction between the Pamir and Tien Shan observed by GPS. *Tectonics* 2016;35:283–92. <https://doi.org/10.1002/2015TC004055>.

Further reading

- [1] Hamada M, Yasuda S, Ioyama R, Emoto K. Study on liquefaction induced permanent ground displacements. Japan: Association for Development of Earthquake Prediction; 1986.
- [2] Huang R, Q, Pei X, J, Li T, B. Basic characteristics and formation mechanism of the largest scale landslide at Daguangbao occurred during the Wenchuan earthquake. *J Eng Geol* 2008;16(6):730–41. [in Chinese, with English abstract].
- [3] Liu Z, J, Wang P, Zhang Z, H, Li Z, G, Cao Z, Z, Zhang J, Y, Yuan X, M, Wang W, Xing X, C. Liquefaction in western Sichuan Basin during the 2008 Mw 7.9 Wenchuan earthquake, China. *Tectonophysics* 2016:1–25.
- [4] Li S, Chen J, B, Wu G, D. Research on characteristics of the geological disaster in the meizoseisma area induced by the Xinyuan-Hejing Ms6.6 earthquake in 2012. *J Seismol Res* 2015;38(3):389–95. [in Chinese, with English abstract].
- [5] Sarma S, K, Ambraseys N. Liquefaction of soils induced by earthquakes. *Bull Seismol Soc Am* 1969;59:651.